Supporting Information

Gainaru et al. 10.1073/pnas.1411620111

Difference in Relaxation Time of ASW and LDA Water

Comparison of relaxation times obtained for LDA water and ASW (Fig. 1) reveals a difference of almost one order of magnitude at the same temperature, with the ASW sample showing slower relaxation for both H-ASW and D-ASW. LDA is a compact material of surface area <1 m^2/g, whereas ASW is a highly microporous, fluffy material with a surface area of several hundred square meters per gram at low temperatures (<77 K) that can efficiently take up impurities from the background gas (1, 2). The network of the micropores in ASW then collapses upon heating to >130 K, and some impurities remain irreversibly trapped within the bulk of ASW (3). This difference in surface-to-volume ratio and some impurities may be at the origin of the observed differences between LDA and ASW (Fig. 1).

Estimates of T_{onset} from Rate-Dependent Dielectric Measurements of LDA

To compare the dielectric results with the DSC measurements the complex permittivity ε^* of protonated and deuterated LDA was recorded not only at constant temperatures (Fig. S2) but, in addition, at a constant frequency of 1 Hz for various heating rates q. In Fig. 2 and Fig. S3 the results for the imaginary part of ε^*, normalized by its maximum value, ε''_{max}, are plotted as a function of temperature. Using a procedure similar to the one used for estimating T_g from calorimetric data, we extracted dielectric onset temperatures, T_{onset}, as the intersection point of the linear increase of $\varepsilon''/\varepsilon''_{max}$ at $T > T_{onset}$ with a baseline, $\varepsilon''/\varepsilon''_{max} = 0$, taken to characterize the loss behavior at low temperatures. The linear increase of ε'' was obtained from a linear fit of the dielectric data in the range $0.5 < \varepsilon''/\varepsilon''_{max} < 0.9$. The resulting fits, extrapolated to $\varepsilon''/\varepsilon''_{max} = 0$, are shown in Fig. 2 and Fig. S3. The error bars for ΔT_{onset} (Fig. 2*G*) account for the small deviations from the linear regression and for deviations occurring when the fitting range varies between $0.3 < \varepsilon''/\varepsilon''_{max} < 0.9$ and $0.7 < \varepsilon''/\varepsilon''_{max} < 0.9$. The data in Fig. S3 also show that the maximum in ε'' vs. T is broad and smooth at high heating rate q. This maximum reflects that the condition $2\pi\nu\tau \sim 1$ is fulfilled before the transformation to the cubic ice phase sets in. This dielectric loss maximum thus signals the presence of a relaxation process. The decay in ε'' observed at higher T gets sharper at heating rates $q \leq 0.2$ K/min, thereby precluding a consistent determination of ε''_{max} (Fig. S3). Thus, the maximum at slow heating rate might not reflect a relaxation maximum, but rather a crystallization-related loss maximum. Hence, we refrain from using the data obtained with heating rates slower than 0.2 K/min in our analysis of ΔT_{onset}.

1. Li J (1996) Inelastic neutron scattering studies of hydrogen bonding in ices. *J Chem Phys* 105(16):6733–6755.
2. Mayer E, Pletzer R (1986) Astrophysical implications of amorphous ice – a microposrous solid. *Nature* 319(6051):298–301.
3. Mitterdorfer C, et al. (2014) Small-angle neutron scattering study of micropore collapse in amorphous solid water. *Phys Chem Chem Phys* 16(30):16013–16020.

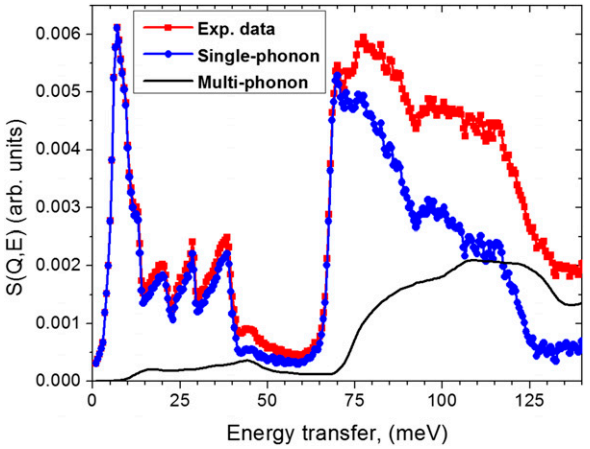

Fig. S1. Dynamical structure factor $S(Q,E)$ for an LDA sample obtained from the INS spectra measured at $T = 15$ K: the experimental spectrum (1) (red curve), calculated multiphonon (black line), and single-phonon (blue curve) contributions.

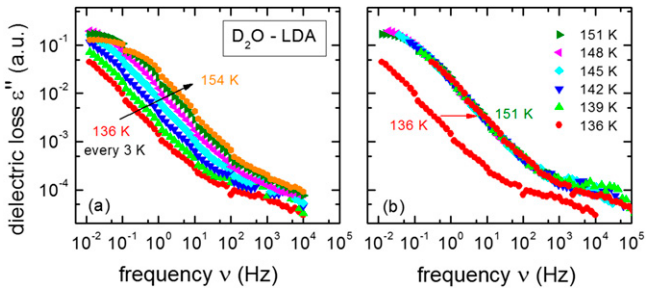

Fig. S2. (*A*) Dielectric loss spectra of deuterated LDA water. (*B*) Master curve obtained by shifting the data in *A* horizontally on top of the spectrum at 151 K. In *B* the (unshifted) dielectric data at 136 K are plotted to demonstrate the scaling procedure.

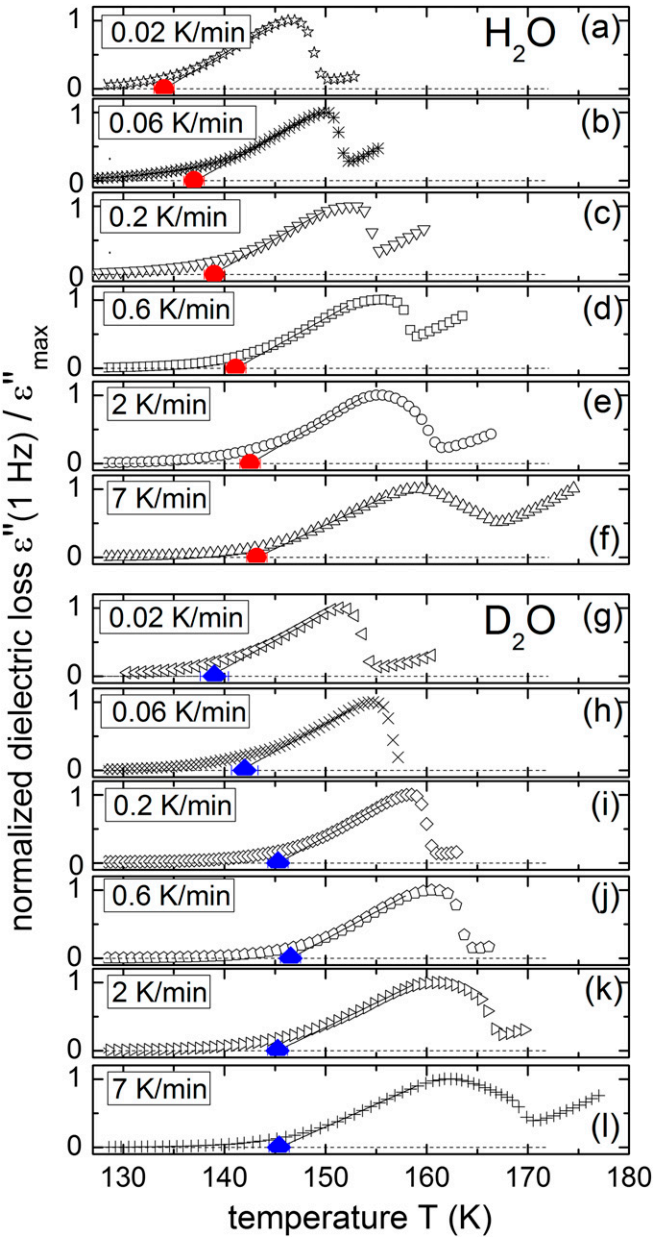

Fig. S3. Temperature dependence of normalized dielectric loss measured at 1 Hz by heating H-LDA (*A*–*F*) and D-LDA (*G*–*L*) at various rates.

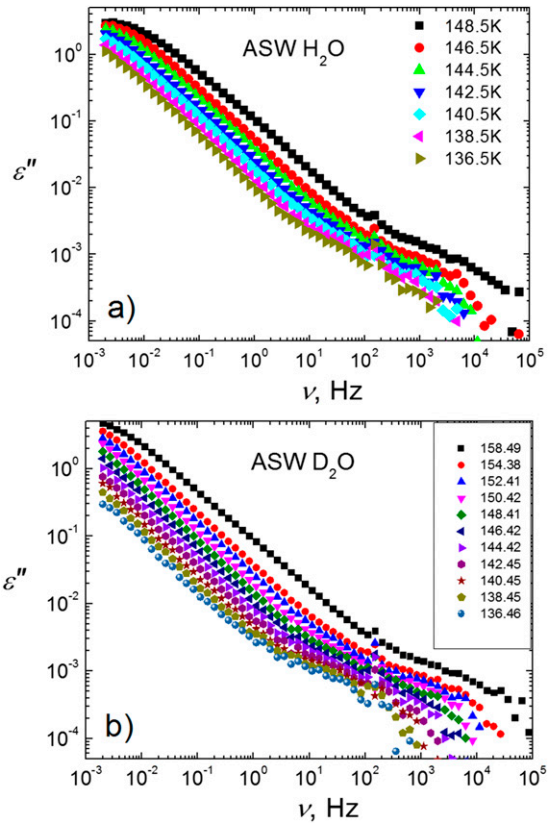

Fig. S4. Dielectric spectra of ASW samples: (*A*) H_2O and (*B*) D_2O.

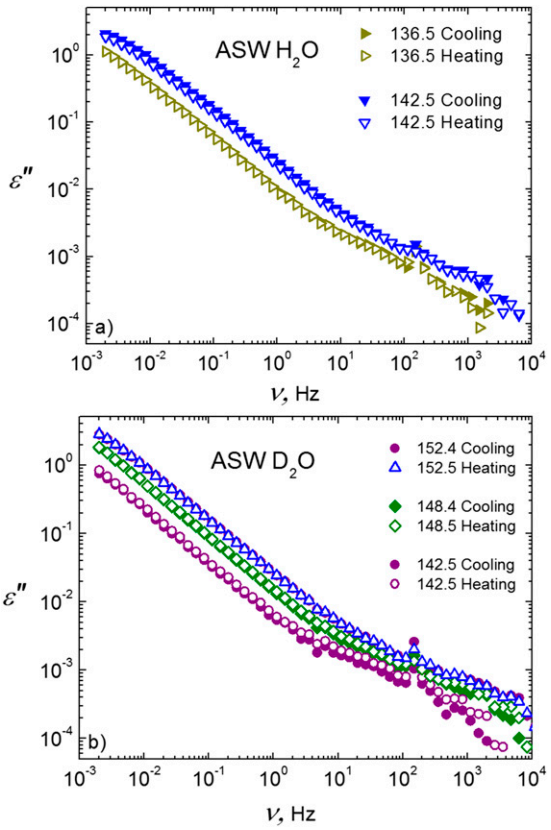

Fig. S5. Dielectric spectra of ASW (*A*) H_2O and (*B*) D_2O samples measured on initial cooling and subsequent heating cycles. The reproducibility of the spectra demonstrates an absence of crystallization.

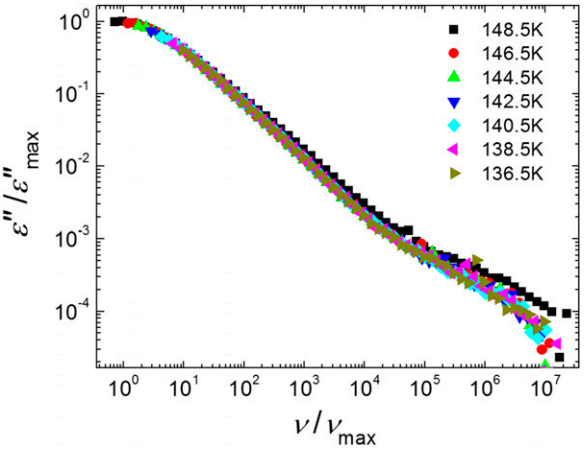

Fig. S6. Time–temperature superposition plot of dielectric relaxation spectra of the ASW-H_2O sample.

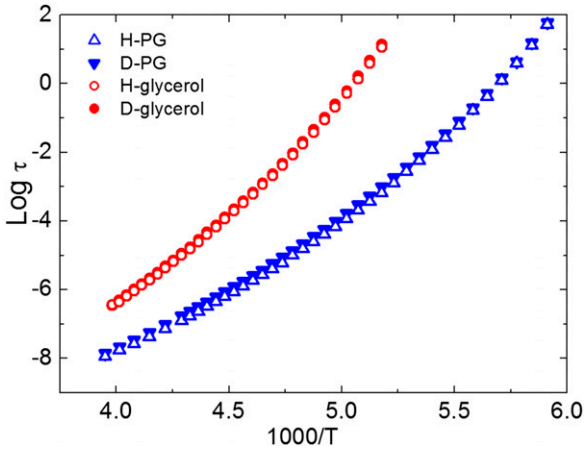

Fig. S7. Structural dynamics in propylene glycol and glycerol. An isotope effect on the glass transition in these hydrogen bonding liquids is very small, $\Delta T_g \approx 0.1$ K for PG and $\Delta T_g \approx 0.4$ K for glycerol (2).